# *TEMPERATURE COEFFICIENTS OF MATERIAL PROPERTIES FOR ELECTRODEPOSITED MEMS*

Larry L. Chu, Long Que, and Yogesh B. Gianchandani*
Department of Electrical and Computer Engineering, University of Wisconsin, Madison, USA


## *ABSTRACT*

This paper presents the use of micromachined differential capacitive strain sensors to investigate mechanical properties of electroplated Ni deposited under two different conditions on Si and glass substrates. The thermal expansion coefficient (α), Young's modulus, and residual strain were studied as a function of temperature. The measured α was 8-16 ppm/K over 23-150°C; the residual strain changed from neutral to –880 microstrain over 23-100°C in one case and +68.5 microstrain to –420 microstrain over 23-130°C in another case; and the Young's modulus ranged from 115-135 GPa at room temperature. The sensitivity of the device to structural non-idealities was evaluated by numerical modeling.


## *I. INTRODUCTION*

Monitoring the mechanical properties of structural materials is a critical challenge in MEMS research and manufacturing. Device performance parameters are sensitive to variations in Young's modulus, residual strain, residual stress, and the thermal expansion coefficient (α) of structural materials. Unfortunately, these properties can vary with manufacturing, packaging, and deployment conditions. It is particularly challenging to control these properties in additive fabrication processes, which require the deposition of the structural material onto the substrate wafer. Specially designed microstructures can often be used for rapid characterization and monitoring processes tolerances of material properties. Additionally, if designed for electronic readout they can be integrated within device packages, improving overall performance by offering post-deployment calibration capability. Many of the mechanical properties of interest can be extracted from a force-deflection measurement. In past efforts electrostatic forces have been used to cause out-of plane deflections of cantilevers, beams, and plates [1-4]. However, a number of sensors and actuators are based on lateral deflections that occur parallel to the plane of the substrate. A laterally deflecting test device is preferred for characterizing the materials used in these devices, which may be anisotropic and may exhibit different properties for in-plane and out-of-plane deflections. The differential capacitive strain sensor [5] is a suitable tool for such measurements. It provides the added benefit of wide dynamic range, accommodating not only tensile strains, but also compressive strains which are sometimes encountered in actuator applications [6].

This paper presents the use of differential capacitive strain sensors to measure the material properties of electroplated Ni, which is often used as a structural material in micromachined devices. Since α for Ni differs significantly from that of Si and glass–two common substrate materials–the measurements are performed over a range of temperatures to determine the temperature coefficients of various properties.

## *II. PROCEDURE*

In the strain sensor a series of ribs, suspended above the substrate by bent-beams, support interdigitated tines, forming sidewall capacitors (Fig.1). The suspensions and tines are arranged such that the capacitance on one side of a rib increases as the other decreases. The residual strain in the structural material is determined from the differential capacitance, $\Delta C = C_{AB} - C_{AC}$, which is >0 in tension, and <0 in compression. The $\Delta C$ is relatively immune to common mode parasitic capacitances. The Young's modulus is determined from the relationship between $C_{AB}$ (or equivalently, $C_{AC}$) and bias voltage between elements A and B (or C). This voltage provides an electrostatic force, resulting in a displacement that is measured by the change in capacitance. The displacement is related to the stiffness of the suspension, which is proportional to the Young's modulus.

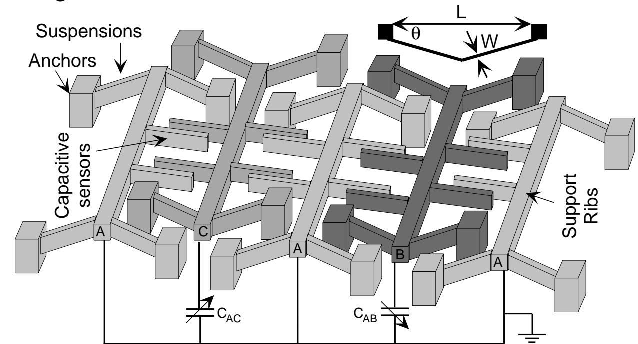


Fig. 1: Schematic of the strain sensor. For tensile materials $\Delta C=C_{AB}-C_{AC}>0$, whereas for compressive materials, $\Delta C<0$

The modeling approach was conceptually similar to those described in [2-4]. The capacitance between tines was numerically modeled using FastCap™ [7]. The capacitance was determined for a range of separations between tines, and stored in a look-up table. The mechanical spring constant of the bent-beam suspensions was calculated as noted in [6]. The compliances of the tines and support rib were added in, resulting in the formula for net mechanical compliance described in Table I. This formula matched FEA simulations for deflection within 10% for the dimensions considered. Next, starting with the zero-bias gap, spacing between the tines was decremented in small intervals. At each position, the capacitance was determined from the look-up table, while the corresponding bias voltage was determined from force balance by equating the electrostatic attractive force to the mechanical restoring force:

$$k_{eff}\, y = \frac{V_{Bias}^2}{2}\frac{\partial C_{AB}}{\partial y} \quad (1)$$

where $k_{eff}$ is the effective mechanical spring constant of the system, and $y$ is the in-plane displacement from the zero-bias position. Figure 2 shows calculated capacitance versus bias

* 1415 Engineering Drive, Madison, WI 53706-1691; Tel: (608) 262-2233, Fax: 262-1267, E-mail: yogesh@engr.wisc.edu

voltage (CV) curves obtained by this method, assuming L=198 µm, W= 5 µm, ø=0.1 rad., 4.4 µm thickness, and 10 pairs of tines exist with 167 µm interdigitated length. The sidewalls of the tines were assumed to have a re-entrant profile that was 22° off vertical. The zero-bias gap between the upper edges of adjacent tines (where the tines were closest) was 1.85 µm. The tines were assumed to be 2.2 µm above the substrate. The compliances of the tines and rib are neglected in this figure.

The effect of certain structural non-idealities on the CV curves is shown in Figs. 3-5. Figure 3 shows variations in the CV curve caused by changing the gap between the tines. The device dimensions are as for Fig. 2, the Young's modulus is 100 GPa, and the gap between the upper edges of the tines is varied from 1.65 µm to 2.05 µm in 0.1 µm increments. Figure 4 shows the impact of changing the sidewall angles of the tines, while Fig. 5 shows the impact of upward and downward deflections of one tine in each pair. Clearly, each of these variables can have an impact on the CV curves.

### *III. EXPERIMENTAL RESULTS*

Surface micromachined strain sensors were fabricated on silicon wafers insulated with 1 µm thick thermal oxide and 0.5 µm thick LPCVD nitride. A 2 µm thick sputtered Ti sacrificial layer was patterned and covered with a Cr/Ni seed layer. The devices were electroplated into a photoresist mold from a nickel sulphamate solution. At 54°C temperature, using 5-10 mA/cm$^2$ current density, a thickness of 4.4 µm was achieved in 9.5 min. The sidewalls of the plated structures were 22° off vertical due to resist reflow during hard bake. The photoresist mold was subsequently stripped and the sacrificial material etched away. Following this, the sample was coated with self-assembled monolayers using ODS [5]. Optical and SEM images of fabricated structures are shown in Fig. 6a,b.

Another set of strain sensors was fabricated on (#7740) glass substrates using LIGA technology [8]. These devices were plated on a 2 µm thick sacrificial layer using a Ni sulphamate solution which had Ni concentration of 82 g/L. At 56°C temperature and 32 mA/cm$^2$ current density, a thickness of 55 µm was achieved in 95 min. (Fig. 6c). The increased thickness provides large sidewall capacitance which improves sensitivity and reduces measurement uncertainty. Thick structures also eliminate out-of-plane deformation and buckling and allow testing at higher temperatures. The LIGA devices also benefit from precise dimensional control and from vertical sidewalls.

The α for Ni was first measured by a passive bent-beam strain sensor [9] which was co-fabricated with the 4.4 µm thick devices. The dimensions of these devices were L= 198 µm, W= 6 µm, and θ= 0.1 rad. Strain was measured as a function of temperature by visually monitoring their deformations and compensating for α for Si, which changes from 2.5 ppm/K at 23°C to 4 ppm/K at 500°C [9]:

$$\alpha_{Metal}(T) = \alpha_{Si}(T) - \frac{d(e(T))}{dT} \qquad (2)$$

where *e(T)* is the strain observed by the strain sensor. The residual strain changed from $1.1\times10^{-10}$ at 23°C to –880 microstrain at 100°C. The α for Ni increased from ≈13.5 ppm/K at 50°C to ≈16.5 ppm/K at 150°C (Fig. 7). This compares well with previously published results. One report indicates that α for Ni increases from 10.2 ppm/K at 20°C to 16.3 ppm/K at 300°C, and holds the latter value at 400°C as well [11]. Another indicates that α for Ni electroplated under particular conditions may increase from 8.5 ppm/K averaged over the temperature range of 25-50°C to 15.1 ppm/K averaged over the temperature range of 25-367°C [12].

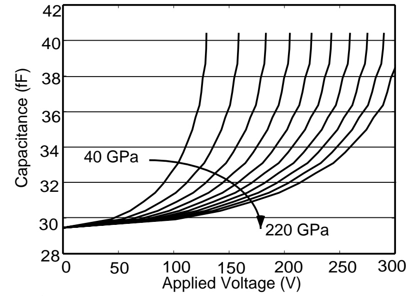


Fig. 2: Theoretical CV curves for Young's moduli of 40-220 GPa in 20 GPa increments.

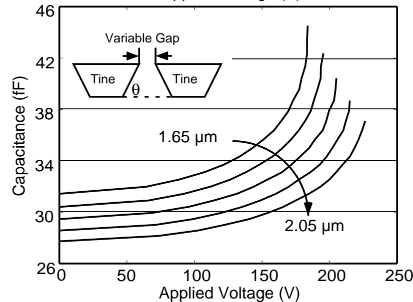


Fig. 3: Impact of gap variations between tines.

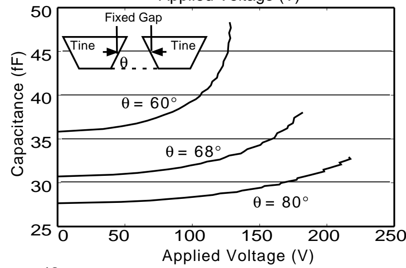


Fig. 4: Impact of variations in the sidewall angles of tines.

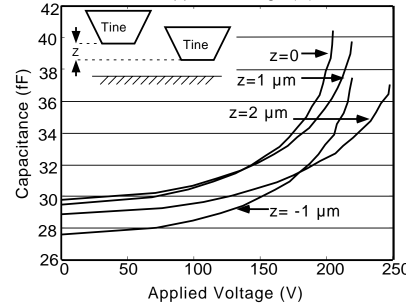


Fig. 5: Impact of out-of-plane deflections of tines.

Capacitive strain sensors were then used to monitor the residual strain in the Ni as a function of temperature (Fig. 8a). Measurements showed a linear increase in differential capacitance from 20°C to 60°C. Measurements were taken with ±0.5 fF precision using a device with 10 tine pairs with 168 µm overlap length and 5 µm nominal gap, suspensions with L=198 µm, W=6 µm, and θ=0.2 rad., and ribs with L= 438 µm and W= 10 µm. The device response to increasing temperature was theoretically estimated using FastCap™, assuming that the average α for Ni exceeds that for Si by 10 ppm/K. This result is superimposed on the measured data in Fig. 8. Based on the passive strain sensor measurements (Fig. 7) and previously published results, the expansion mismatch between nickel and

silicon over 20-60°C was 6-11 ppm/K, consistent with the differential capacitance measurements. At temperatures >60°C, however, the 4.4 µm thick devices were affected by out-of-plane buckling of the support ribs. This suggests dimensional constraints for future designs.

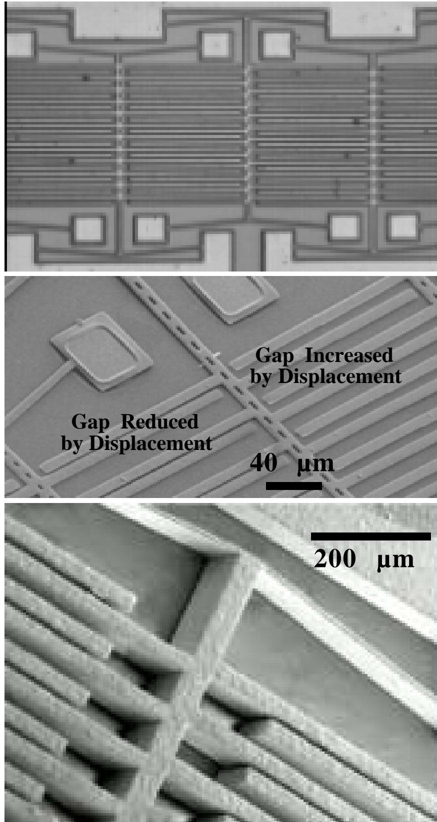


Fig. 6: (a-upper) Optical image of a 4.4 µm thick strain sensor; (b-center) SEM of a released 4.4 µm thick device showing displaced tines. All tine spacings were equal before release; (c-lower) SEM of a released 55 µm thick strain sensor.

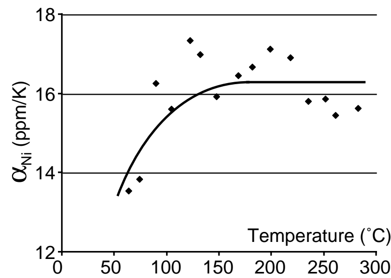


Fig. 7: The α for electro-plated Ni, as measured by passive bent-beam strain sensors.

The ΔC measurements of a LIGA device indicated that the residual strain was +68.5 microstrain at 23°C and -236 microstrain at 85°C. These values were determined by fitting the measured ΔC to calculated values using the procedure outlined in the preceding section. This device had 24 tines in each of four banks, with 900 µm overlap length, 1040 µm total length, 29 µm width, and 10 µm nominal gap; suspensions with L= 1000 µm, W= 10 µm width, and θ= 0.1 rad.; and ribs with L= 2550 µm and W= 45 µm. After accounting for the α for glass which is 3.25 ppm/K [9], these measurements indicate that α for Ni that was plated for the LIGA devices was 8.2 ppm/K when averaged over 23-85°C, which falls within the range previously reported [12]. Further confirmation of this was obtained by using the change in $C_{AC}$ alone as a function of temperature. The calculated and measured capacitances were referenced to the $C_{AC}$ at 37°C, which was the interpolated zero-stress temperature (Fig. 8b). The fit indicates that α for Ni was 7.9 ppm/K. At 130°C the calculated increase in the gap between the tines (with respect to the zero-stress position) was 3.95 µm, corresponding to a residual strain of –420 microstrain. This matched with the calibrated visual measurement of ≈3.7 µm.

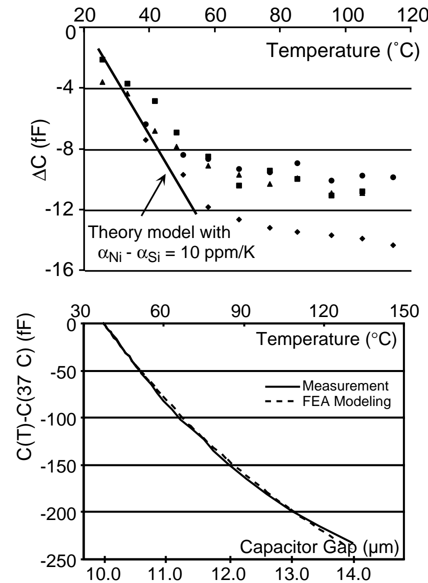


Fig. 8: (a-upper) The expansion coefficient measured capacitively for four adjacent devices. $T_{buckle}$≈60°C. (b-lower) Capacitance change referenced to the neutral position for a LIGA device. No buckling.

Figure 9a shows CV curves that were measured at various temperatures for 4.4 µm thick devices with dimensions as noted previously, except θ= 0.1 rad. Numerically simulated curves were fitted to measurements using the zero bias capacitance and the Young's modulus as fitting parameters. A comparison of a measured and fitted curve pair is shown in Fig. 9b. The best fit of $k_{eff}$ corresponded to a Young's modulus of 135±15 GPa at 23°C for the electroplated metal. Measurements for the LIGA device are plotted in Fig. 10 as fractional changes in measured capacitance as a function of $V^2$. In this representation, the *y*-axis is proportional to the fractional change in the gap between the tines, while the *x*-axis is proportional to the electrostatic force. At 23°C the best fit corresponds to a Young's modulus of 115±10 GPa. Some of the uncertainty is attributable to the calculation of fringing fields and the impact of parasitics in measurements. These were eliminated from the strain measurements because ΔC was used instead of $C_{AC}$. Consequently, it may be possible to reduce the uncertainty by using ΔC•V measurements (Fig. 11). This possibility is being investigated. Although the Young's modulus of bulk nickel is 208 GPa, electroplated nickel has a substantially lower modulus and can demonstrate significant variability, underscoring the need for such measurements. For Ni electroplated under particular conditions, a value of 150 GPa was reported in [13]. Trace levels of contamination and variations in plating conditions can significantly affect the mechanical properties of electroplated materials. An XEDS plot of the 4.4 µm thick plating sample is shown in Fig. 12.

Both the 4.4 µm thick and 55 µm thick devices showed that the Young's modulus decreased with increasing temperature. This is also evident from the trend in Fig. 10. The temperature coefficient of the Young's modulus, which is the same as that of

$k_{eff}$, was estimated as -1590 ppm/K. There is significant uncertainty in this value because measurement and fitting errors are compounded. This parameter is also strongly dependent on fabrication conditions, and values ranging from -550 ppm/K [13] to -952 ppm/K [11] have been reported previously.

Using the measured values of strain and Young's modulus the thermal stress in the metal microstructures can be calculated in a piecewise linear manner. For the plating solution and conditions used in the 4.4 μm thick devices, at 23°C the stress is essentially zero, and at 100°C it is approximately –105 MPa.

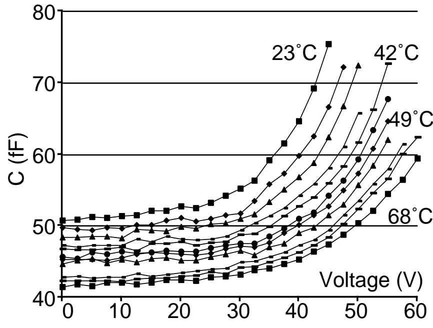


Fig. 9: (a-upper) Measured CV as a function of temp. for a 6 μm thick device with $T_{buckle}$>70°C.

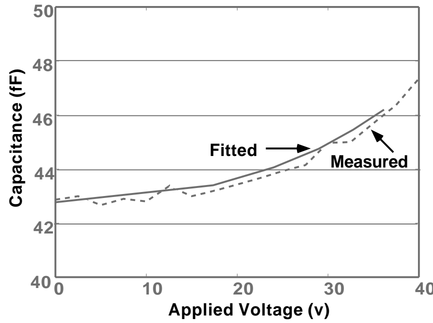


(b-lower) Comparison of a measured CV curve from Fig. 9 to a fitted theoretical one at T =60°C.

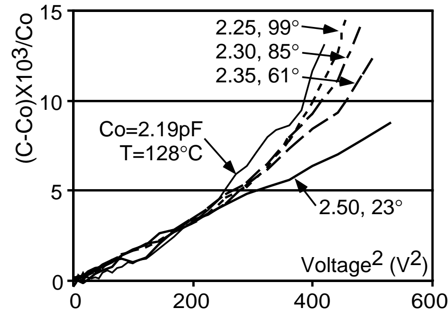


Fig. 10: Measured $C_{AC}$V of 55 μm thick strain sensors at various temps.

## IV. CONCLUSIONS

In summary, a procedure for determining temperature dependent mechanical properties of electrodeposited metals using differential capacitive strain sensors has been described and evaluated in the context of Ni microstructures electroplated under different conditions and from different solutions on Si and glass substrates. For the fabrication conditions used, it was found that the α for Ni was 8-16 ppm/K over 23-150°C; the residual strain changed from neutral to –880 microstrain over 23-100°C in one case and +68.5 microstrain to –420 microstrain over 23-130°C in another case; and the Young's modulus ranged from 115-135 GPa at room temperature, and had an estimated temperature coefficient of about -1590 ppm/K. Theoretical calculations indicate that CV measurements can be affected by variations in device dimensions. However, when these are known *a-priori*, the measurements of material properties provided by differential capacitive strain sensors are consistent with expectations.

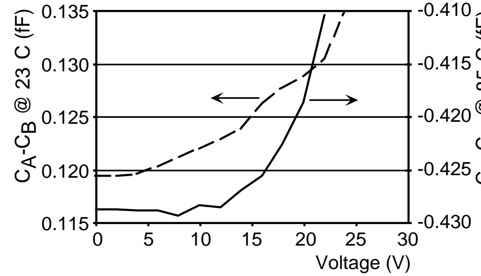


Fig. 11: Measured ΔC•V of 55 μm thick strain sensors at two temps.

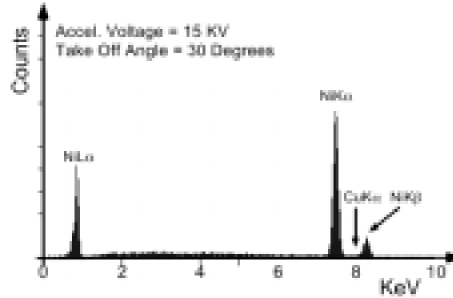


Fig. 12: XEDS plot showing <0.1% Cu contamination in the Ni film.

**Acknowledgements**: The authors are grateful to the late Prof. H. Guckel and Dr. B. Chaudhuri for helpful discussions.

### *REFERENCES*

[1] K. Najafi, K. Suzuki, "A novel technique and structure for the measurement of intrinsic stress and Young's modulus of thin films," *Intl. Workshop on Micro Electro Mechanical Systems*, 1/89, pp. 96-7

[2] B.E. Artz, L.W. Cathey, "A finite element method for determining structural displacements resulting from electrostatic forces," *Solid-State Sensor & Actuator Workshop,* Hilton Head, SC, 1992, pp. 190-3

[3] P.M. Osterberg, S.D. Senturia, "M-TEST: A test chip for MEMS material property measurement using electrostatically actuated test structures," *IEEE J. Microelectromech. Sys.,* 6(2), 6/97, p. 107-118

[4] E.K. Chan, K. Garikipati, R.W. Dutton, "Characterization of contact electromechanics through capacitance-voltage measurements and simulations," *IEEE J. Microelectromech. Sys.,* 8(2), 6/99, p. 208-217

[5] L. Que, M.-H. Li, L. Chu, Y.B. Gianchandani, "A micro machined strain sensor with differential capacitive readout," *IEEE Intl. Conf. on Micro Electro Mechanical Systems,* Orlando, FL, 1/99, pp. 552-7

[6] J.-S. Park, L.L. Chu, E. Siwapornsathain, A.D. Oliver, Y.B. Gianchandani, "Long throw and rotary output electro-thermal actuators based on bent-beam suspensions," *IEEE Intl. Conf. on Micro Electro Mechanical Systems,* Miyazaki, Japan, Jan. 2000

[7] K. Nabors, S. Kim, J. White, S. Senturia, *FastCap User's Guide,* M.I.T., Sep. 92; also K. Nabors, S. Kim, J. White, *IEEE Trans. Microwave Theory and Techniques,* 40(7), pp. 1496-1506, July 1992

[8] H. Guckel, "High-aspect ratio micromachining via deep X-ray lithography," Proc. of IEEE, 86(8), Aug. 1998, pp. 1586-1593

[9] Y.B. Gianchandani, K. Najafi, "Bent-beam strain sensors," *Journal of Microelectromechanical Systems,* 5(1), pp. 52-58, Mar. 1996

[10] W.H. Ko, J.T. Suminto, G.J. Yeh, "Bonding techniques for micro sensors," *Micromachining & Micropackaging of Transducers,* Elsevier '85; also*Microsensors*, pp. 198-208, *Ed.* Muller *et al,* IEEE Press, '90

[11] E.M. Wise, R.H. Schaeffer, "The properties of pure nickel – I," *Metals and Alloys,* Sep. 1942, pp. 424-428

[12] J.W. Dini, H.R. Johnson, "Coefficient of thermal expansion of sulphamate nickel electrodeposits," *J. Materials Sc.,* (10)7, 1975

[13] M. Putty, *A micromachined vibrating ring gyroscope,* Ph.D. Thesis, Univ. of Michigan, Ann Arbor, pp. 211-212, Mar. 1995

Table I: Mechanical compliance of the strain sensor.

$$k_{eff} = [(2 \cdot k_{bb}) \perp (N \cdot k_{tine}) \perp k_{rib}]/2$$

$$k_{bb} = \frac{4 \cdot W_{bb} \cdot H \cdot E \cdot \sin^2 \phi}{L_{bb}} \quad k_{tine} = \frac{2 \cdot E \cdot H \cdot W_{tine}^3}{3 \cdot L_{tine}^3} \quad k_{rib} = \frac{2 \cdot E \cdot H \cdot W_{rib}^3}{L_{rib} \cdot (L_{tine} - 0.5 \cdot L_{ov})^2}$$